Research Square

Preprints are preliminary reports that have not undergone peer review.
They should not be considered conclusive, used to inform clinical practice,
or referenced by the media as validated information.

Electrode degradation during a chemical/mechanical accelerated stress test of membranes in polymer electrolyte membrane fuel cells

Yejun Han
Sunchon National University
Donggeun Yoo
Sunchon National University
Sohyeong Oh
Sunchon National University
Sunggi Jung
SANG-A FRONTEC CO. Ltd
Jun Sub Lee
SANG-A FRONTEC CO. Ltd
Kwonpil Park
parkkp@sunchon.ac.kr

Sunchon National University https://orcid.org/0000-0001-6634-4402

Research Article

Keywords: PEMFC, AST, OCV-Wet/Dry, Electrode Degradation, Shorting

Posted Date: November 4th, 2026

DOI: https://doi.org/10.21203/rs.3.rs-11336455/v1

License: This work is licensed under a Creative Commons Attribution 4.0 International License.
Read Full License

Electrode degradation during a chemical/mechanical accelerated stress test of membranes in polymer electrolyte membrane fuel cells

Yejun Han[1], Donggeun Yoo[2*], Sohyeong Oh[2], Sunggi Jung[3], Jun Sub Lee[3] and Kwonpil Park[1,2*]

[1] Department of Chemical Engineering, Sunchon National University 255, Jungang-ro, Suncheon-si, Jeonnam-Gwangju, 57922, Republic of Korea.

[2] Renewable Energy Evaluation Center, Sunchon National University 255, Jungang-ro, Suncheon-si, Jeonnam-Gwangju, 57922, Republic of Korea.

[3] SANG-A FRONTEC CO.Ltd, 369 Route 18, Namdong-ro, Namdong-gu, Incheon, 21629, Republic of Korea.

* Corresponding author. E-mail: parkkp@scnu.ac.kr (Kwonpil Park) and ehdrms6832@gmail.com (Donggeun Yoo)

Donggeun Yoo and Kwonpil Park contributed equally to this work.

Abstract

Improving the durability of polymer electrolyte membrane fuel cells requires a comprehensive understanding of membrane and electrode degradation. Although the U.S. Department of Energy introduced the OCV-Wet/Dry Cycle as a protocol for evaluating membrane durability, the voltage fluctuations occurring during this process also induce electrode degradation. This study investigated electrode degradation and its effects on membrane durability during 6,000 OCV-Wet/Dry cycles. The electrochemically active surface area (ECSA) decreased by approximately 50%, and the short-circuit resistance decreased to 0.5 kΩ·cm^2, at which point the test was terminated. Up to 5,000 cycles, the open-circuit voltage (OCV) exhibited reversible fluctuations, and the hydrogen crossover current density (HCCD) remained nearly constant. Beyond 5,000 cycles, irreversible OCV fluctuations emerged, accompanied by an approximately fivefold increase in the ECSA degradation rate and a sharp rise in HCCD. Transmission electron microscopy and X-ray diffraction revealed a 1.7–1.8-fold increase in Pt catalyst particle size. Electrochemical impedance spectroscopy and distribution of relaxation

times analysis, together with thermal imaging, indicated that catalyst degradation was associated with shorting and accelerated membrane degradation. These results indicate that the OCV-Wet/Dry Cycle is more appropriately regarded as a protocol that induces coupled degradation of both the electrodes and the membrane in the MEA.

Keywords

PEMFC, AST, OCV-Wet/Dry, Electrode Degradation, Shorting

1. Introduction

With increasing concerns over greenhouse gas emissions from fossil fuel consumption and climate change, growing attention has been directed toward environmentally sustainable energy technologies that can replace conventional fossil fuels [1]. Proton exchange membrane fuel cells (PEMFCs) generate electrical energy through the electrochemical oxidation of hydrogen and the reduction of oxygen, while protons are transported through the polymer electrolyte membrane [2]. Due to their low operating temperature, fast startup, and high power density, PEMFCs have been widely studied for various applications, including hydrogen-powered vehicles and small scale power generation systems [2, 3].

However, PEMFCs still face several technical challenges that need to be addressed. Representative issues include performance degradation and durability problems during long-term operation, as well as water management within the electrodes and polymer electrolyte membrane [3, 4]. Because these issues directly affect the efficiency, lifetime, and economic feasibility of fuel cells, various studies have been actively conducted to address them [3]. Although research on the membrane electrode assembly (MEA) required to achieve the performance of PEMFCs has continued to advance, durability problems during long-term operation remain a challenge [3, 4]. For heavy-duty vehicles, the durability target is set at

30,000 h. However, even under accelerated stress conditions designed to simulate actual operating conditions, the durability target is often not achieved because of MEA degradation before reaching the equivalent operating time [5, 6]. Therefore, understanding the MEA degradation mechanisms that occur during accelerated stress test (AST) is very important for improving the durability of PEMFCs [3, 5, 6].

PEMFC MEA degradation can generally be classified into electrode degradation and membrane degradation. Electrode degradation involves the deterioration of the Pt catalyst, carbon support, and ionomer binder within the catalyst layer. In the case of Pt, particle growth occurs through dissolution and redeposition processes. Degradation of the carbon support, primarily caused by carbon oxidation, can lead to structural collapse of the catalyst layer and promote Pt particle coalescence, thereby accelerating catalyst particle growth [7]. Degradation of the ionomer binder can also contribute to the structural deterioration of the catalyst layer. Consequently, degradation of these electrode components results in a reduction in the electrochemical active surface area (ECSA). Membrane degradation can be categorized into electrochemical degradation caused by radical attack and mechanical degradation induced by stresses associated with repeated wet/dry cycling [8]. Degradation of the electrolyte membrane ultimately increases hydrogen permeability through the membrane and may eventually lead to membrane failure.

Various durability evaluation methods have been developed to assess the durability of the electrodes and the electrolyte membrane in PEMFC [9, 10]. However, durability test performed under actual PEMFC operating conditions may require thousands to tens of thousands of hours. Therefore, various accelerated stress test (AST) protocols have been investigated to shorten the evaluation time while reproducing the MEA degradation.

For electrode degradation ASTs, a potentiostat is typically used to control the electrode potential depending on the target material for degradation, thereby inducing Pt oxidation and

reduction or carbon oxidation. Electrolyte membrane degradation ASTs include OCV holding and wet–dry cycling, which are used to induce electrochemical and mechanical degradation of the membrane, respectively. In 2016, the U.S. Department of Energy (DOE) proposed the OCV-Wet/Dry cycle to simultaneously evaluate the chemical and mechanical durability of polymer electrolyte membranes. The protocol is an effective approach for accelerating membrane degradation because it simultaneously induces mechanical and chemical degradation of the polymer electrolyte membrane. However, during the combined OCV holding and wet/dry cycling processes, voltage fluctuations occur at the cathode, which can induce electrode degradation. Despite this potential for electrode degradation, the effects of OCV Wet/Dry cycle on electrode degradation have not yet been investigated.

In this study, electrode degradation during a chemical/mechanical accelerated stress test (AST) was investigated using the OCV Wet/Dry Cycle as the durability evaluation protocol. Electrochemical characterization was performed using cyclic voltammetry (CV), linear sweep voltammetry (LSV), and electrochemical impedance spectroscopy (EIS), with distribution of relaxation times (DRT) analysis used to elucidate the contributions of different electrochemical processes to performance degradation. In addition, postmortem analyses, including X-ray diffraction (XRD), scanning electron microscopy (SEM), and transmission electron microscopy (TEM), were conducted to examine membrane and catalyst degradation in the MEA.

2. Experimental

2.1. MEA Specifications and Electrochemical Accelerated Degradation Evaluation Methods

The MEA was fabricated by hot-pressing electrodes with a Pt loading of 0.4 mg cm^{-2} onto both the anode and cathode sides of a Nafion 211 membrane (25 μm thick; Chemours, USA). The MEA was assembled into a unit cell with an active area of 25 cm^2 using a gas diffusion

layer (Sigracet 39BB, SGL Carbon, Germany).

The AST was conducted using the OCV wet/dry cycle, with an accelerated degradation protocol applied beyond the conditions proposed by the U.S. Department of Energy (DOE). The OCV-Wet/Dry Cycle consists of repeated humidification of the cell at 100% relative humidity (RH) for 60 s at 90 °C, followed by drying at 0% RH for 60 s. During the cycling, H_2 and air were supplied to the anode and cathode, respectively, at a flow rate of 2 L min^{-1}. Characterization was performed every 1,000 cycles, and the test was terminated when the short-circuit resistance (SR) decreased below 1 kΩ cm^2.

2.2. MEA Characterization

All characterization was performed at a cell temperature of 70 °C and 100% RH. The I–V polarization curves were measured at stoichiometric ratios of 1.5 and 2.0 for the anode and cathode, respectively. The cell temperature, gas flow rates, and relative humidity were controlled using a fuel cell evaluation system (CNL, Korea).

2.2.1 Cyclic Voltammetry

CV measurements were conducted using a potentiostat (SI 1287, Solartron, Germany) at a scan rate of 30 mV s^{-1} for 15 cycles. The potential range was 0.05–1.2 V. During the measurements, hydrogen and argon were supplied to the anode and cathode at flow rates of 40 mL min^{-1} and 200 mL min^{-1}, respectively.

ECSA was calculated by integrating the hydrogen desorption region in the potential range of 0–0.4 V in the CV and applying a conversion factor of 210 μC cm^{-2}. The equation used to calculate the ECSA is as follows:

$$\frac{H_2 \text{ desorption area (mV mA cm}^2\text{)}}{210\ (\mu C\ cm^{-2}) \times \text{scan rate (mV s}^{-1}\text{)} \times \text{Pt loading (mg cm}^{-2}\text{)}}$$

2.2.2 Linear Sweep Voltammetry

LSV measurements were conducted using a potentiostat (SI 1287, Solartron, Germany) at a

scan rate of 1 mV s^{-1} over a potential range of 0.05–0.5 V. During the measurements, hydrogen and argon were supplied to the anode and cathode at flow rates of 40 mL min^{-1} and 200 mL min^{-1}, respectively. SR was calculated as the reciprocal of the slope of the trend line in the potential range of 0.4–0.5 V.

2.2.3 Electrochemical Impedance Spectroscopy and Distribution of Relaxation Times

The EIS measurements were conducted by operating the cell at a current density of 40 mA cm^{-2} using an impedance analyzer (HCP-803, BioLogic, France), with a sinusoidal sweep over a frequency range from 100 kHz to 0.01 Hz.

DRT analysis was performed using DRT Tools [11]. The relationship between the impedance, $Z(\omega)$, and the distribution of relaxation times, $\nu(\tau)$, is given as follows.

$$Z(\omega) = R_{ohm} + \int_0^\infty \frac{\gamma(\tau)}{1 + j\omega\tau} d\tau$$

The analyzed EIS spectra were separated into individual resistive components according to the method reported in [12].

2.3 Postmortem Analysis

2.3.1 X-ray Diffraction (XRD)

The cathode surface of the MEA was analyzed using an X-ray diffractometer (D8 Discover, Bruker). Cu Kα radiation (λ = 1.542 Å) was used as the X-ray source. The particle size was calculated using the Scherrer equation.

2.3.2 Scanning Electron Microscopy and Transmission Electron Microscopy

The cross-sectional thickness and structure of the MEA cathode layer were analyzed using a field-emission scanning electron microscope (JSM-7100F, JEOL, Japan). The MEA was coated with gold and analyzed at an accelerating voltage of 5 kV.

The structure of the Pt/C particles in the cathode layer was analyzed using a field-emission

transmission electron microscope (JSM-F200, JEOL, Japan). The cathode catalyst layer was treated with ethanol and scraped off using tweezers. The collected catalyst layer was then dispersed in ethanol using an ultrasonic disperser, followed by transmission electron microscopy analysis.

2.3.3 Thermal Imaging Camera Analysis

An infrared camera (FLIR A300, Sweden) was used to identify areas where the temperature increased due to shorting. After the degraded MEA was separated from the cell, the MEA and GDL were fixed in a flange cell. The cathode side of the flange cell was exposed to ambient air, while the anode side was maintained under a hydrogen atmosphere. Thermal imaging analysis was performed at room temperature.

3. Results

3.1. Voltage Changes during OCV-Wet/Dry Cycle

Fig. 1 shows the changes in OCV during the OCV–Wet/Dry Cycle. During the OCV–Wet/Dry Cycle, when the condition changes from wet to dry, the OCV initially increases due to a decrease in hydrogen permeability through the membrane [13]. Subsequently, as the effect of reduced water content in the catalyst layer becomes more significant, the activity of the binder ionomer decreases, resulting in a decrease in OCV. During the subsequent wetting process, the activity of the binder ionomer is recovered due to humidification, causing the decreased OCV to rapidly recover. Thereafter, the OCV gradually decreases as the hydrogen permeability increases due to the increased water content in the polymer electrolyte membrane [14, 15].

Fig. 1a shows that the HOL (High OCV Line) and LOL (Low OCV Line) gradually decreased after 5,000 cycles, while the gap between the two lines increased without recovery

during the subsequent cycles. This indicates the occurrence of irreversible degradation. The irreversible degradation is attributed to the degradation of the catalyst layer and polymer electrolyte membrane, involving the combined effects of irreversible electrode degradation caused by an increase in the amount of dissolved Pt, chemical degradation of the membrane caused by radicals, and mechanical degradation of the membrane caused by repeated contraction and expansion [16].

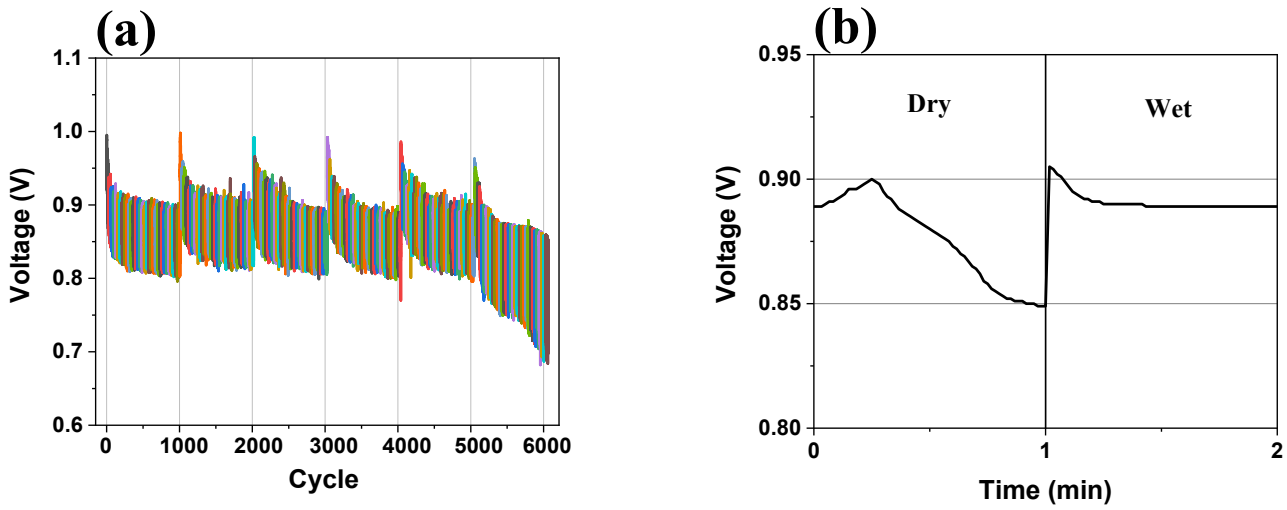


Fig. 1. OCV-Wet/Dry Cycling protocol: (a) overall cycling sequence and (b) a single OCV-Wet/Dry Cycle

3.2. Changes in HCCD and SR during the OCV–Wet/Dry Cycle

Fig. 2 shows the changes in HCCD and SR during the OCV-Wet/Dry Cycle. The LSV remained relatively constant up to 5,000 cycles, and no significant changes were observed, HCCD also remained relatively constant. However, after 5,000 cycles, HCCD increased approximately fourfold, which led to a rapid decrease in OCV (Table 1). This sharp increase in HCCD and decrease in OCV indicate that the polymer electrolyte membrane of the MEA underwent mechanical and chemical degradation. As HCCD increased significantly, the voltage fluctuations during the OCV-Wet/Dry Cycle became more pronounced (Fig. 1a),

primarily due to a decrease in the LOL. The increase in HCCD and the decrease in OCV are considered to be attributable to irreversible degradation of the polymer electrolyte membrane caused by radical attack and the resulting membrane thinning [17-19].

Fig. 2c shows the changes in SR during the OCV–Wet/Dry Cycle. The SR decreased sharply at 5,000 cycles, and the durability evaluation was terminated at 6,000 cycles when the SR reached 0.545 kΩ cm^2, which was below the DOE durability evaluation termination criterion of 1 kΩ cm^2 (Table 1). The occurrence and location of shorting were identified using an infrared camera, as shown in Fig. 8.–

Shorting may occur through electron transport across the membrane involving Pt deposited within the membrane. As catalyst degradation progresses, Pt can dissolve from the catalyst layer and precipitate within the membrane, where it may provide pathways for electron transport. This can increase the short-circuit current and promote localized membrane degradation, including membrane thinning, pinhole formation, and cracking, resulting in a local temperature increase. Consequently, HCCD increased sharply while SR decreased, indicating the progression of severe membrane degradation and shorting [13, 20-22].

Table 1. Variation in OCV, current density at 0.6 V, HFR, CTR, ECSA, HCCD, and SR during OCV-Wet/Dry Cycling

Time (Cycle)	OCV (V)	Current density at 0.6 V (mA cm^{-2})	HFR (mΩ cm^2)	CTR (mΩ cm^2)	ECSA (m^2 g^{-1})	HCCD (mA cm^{-2})	SR (kΩ cm^2)
Pristine	**0.953**	**1204.0**	**69.5**	**1035.5**	**40.1**	**1.541**	**3.998**
1,000	**0.942**	**1014.6**	**69.5**	**1152.8**	**35.8**	**1.485**	**7.153**
2,000	**0.940**	**942.7**	**74.9**	**1218.4**	**33.8**	**1.336**	**7.138**
3,000	**0.940**	**922.1**	**90.0**	**1335.1**	**32.3**	**1.332**	**8.889**

4,000	0.942	878.1	92.3	1335.9	30.9	1.366	14.347
5,000	0.941	842.7	95.0	1418.0	29.5	1.478	3.723
6,000	0.904	851.1	84.6	1159.1	20.8	9.052	0.545

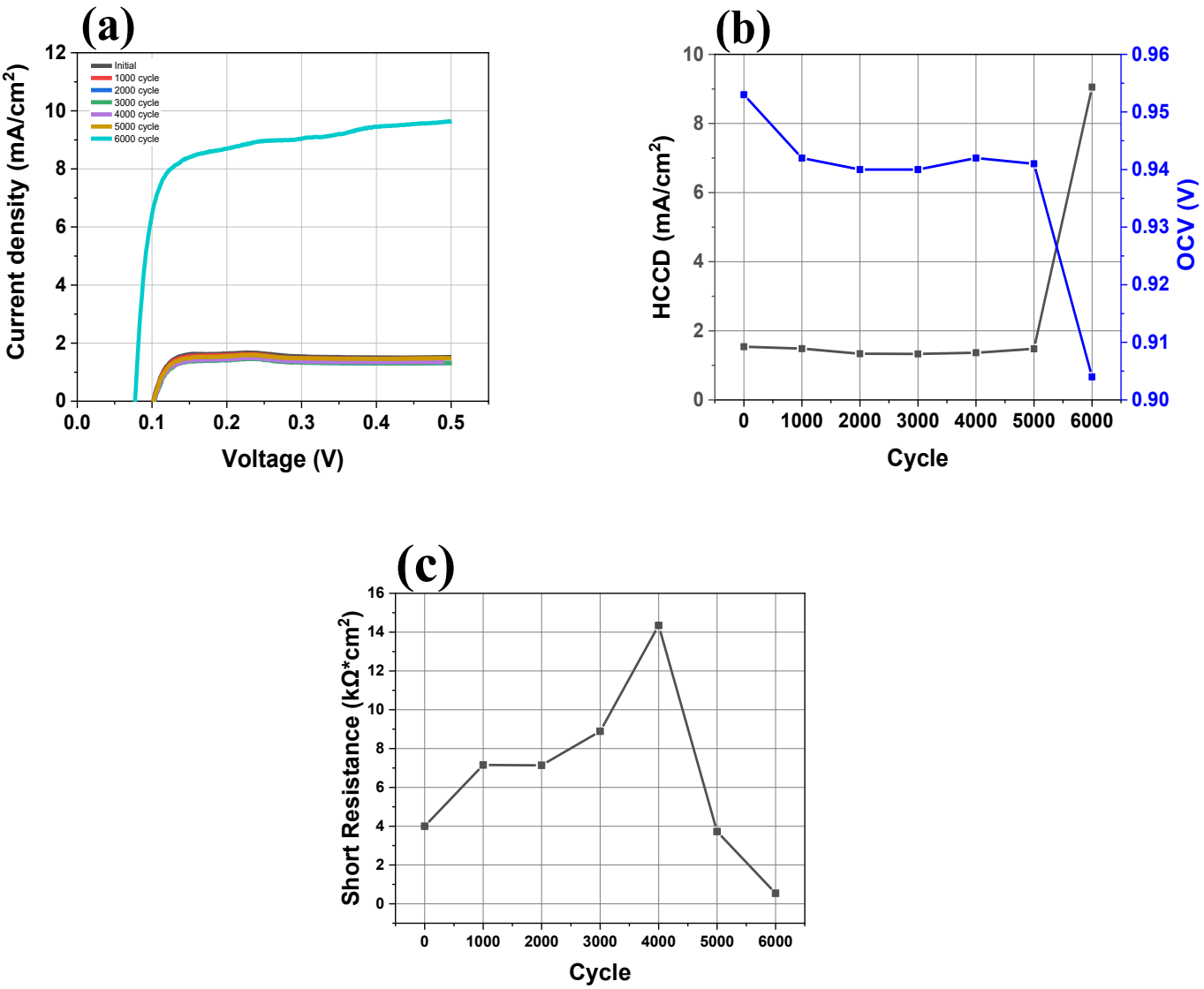


Fig. 2. Variation in (a) LSV, (b) HCCD and OCV, and (c) short-circuit resistance during OCV-Wet/Dry Cycling

3.3. Decrease in ECSA Due to Catalyst Degradation

Fig. 3 shows the changes in CV and ECSA during the OCV-Wet/Dry Cycle. As shown in Fig.

3a, the shape of the CV curve changed progressively during AST, with a pronounced change observed at 6,000 cycles. The ECSA gradually decreased up to 5,000 cycles and then decreased sharply at 6,000 cycles, indicating progressive degradation of the Pt catalyst (Fig. 3b). Catalyst degradation in PEMFCs is predominantly associated with the dissolution and redeposition of Pt catalyst particles, including mechanisms such as Ostwald ripening and Pt dissolution. Direct Pt dissolution generally occurs at high electrode potentials above the OCV, typically around 1.188 V [23]. However, several studies have reported that Pt dissolution can also occur at potentials near the OCV through the reactions described in Equations (1) and (2). During this process, oxidized Pt species are reduced and simultaneously dissolved into the electrolyte as Pt^{2+} ions. The dissolved Pt ions can subsequently migrate toward the membrane and be reduced by hydrogen crossing over from the anode, resulting in Pt precipitation within the membrane, as described in Equation (3) [24, 25].

$$Pt + H_2O \rightarrow PtO + 2H^+ + 2\,e^- \qquad (1)$$

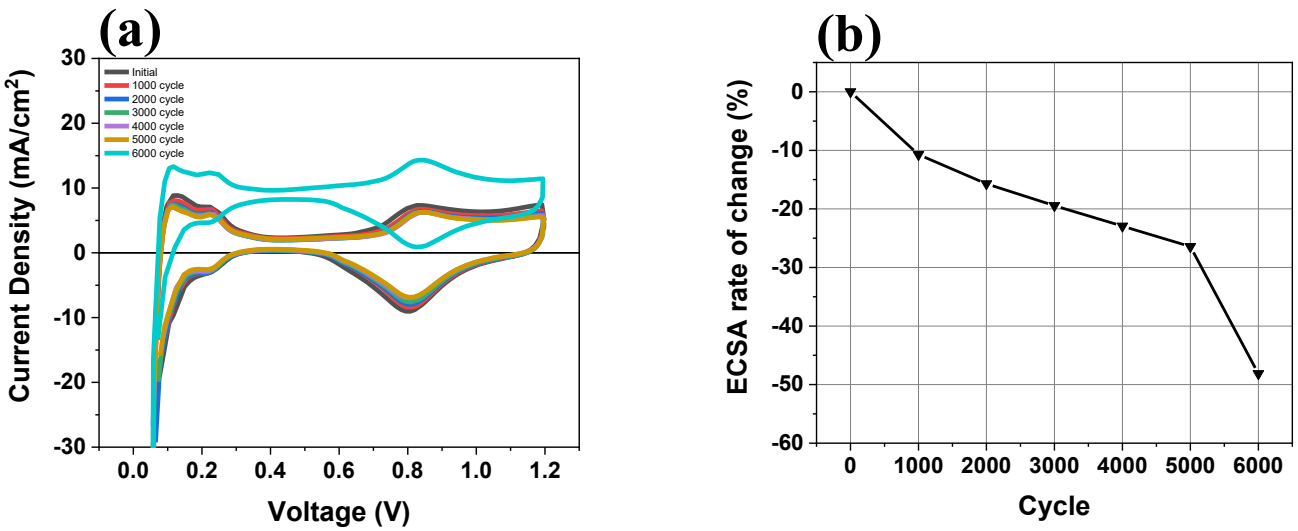
$$PtO + 2\,H^+ \rightarrow Pt^{2+} + H_2O \qquad (2)$$

$$Pt^{2+} + H_2 \rightarrow Pt + 2H^+ \qquad (3)$$

At 6,000 cycles, the ECSA loss exceeded the DOE catalyst AST target of 40%, whereas the HCCD remained below the membrane chemical degradation target of 15 mA cm^2. These results indicate that the catalyst degradation criterion based on ECSA was reached earlier than the membrane chemical degradation criterion based on HCCD. Therefore, significant electrode catalyst degradation was observed during the OCV-Wet/Dry Cycle even before the membrane reached the DOE chemical degradation criterion. Meanwhile, the decrease in SR below 1 kΩ cm^2 indicates that localized membrane failure and shorting progressed during the test, which were likely associated with the migration and deposition of Pt within the membrane resulting from catalyst degradation.

Figs. 3c and 3d compare the changes in OCV and current density at 0.6 V obtained from the

I-V polarization curves measured during the OCV-Wet/Dry Cycling test. The decrease in OCV observed in the I-V polarization curves can be attributed to several factors, including the cathode mixed potential, proton activity in the binder ionomer, hydrogen crossover, and short-circuit current. These factors can be associated with irreversible degradation of the electrodes and membrane [26-28]. A sharp decrease in OCV was observed after 5,000 cycles, indicating that the increase in short-circuit current had a significant influence on the OCV loss. In contrast, the current density at 0.6 V at 6,000 cycles, despite the increased short-circuit current, remained comparable to that measured at 5,000 cycles. This behavior suggests that the shorting occurred locally and therefore had only a limited influence on the overall cell performance.



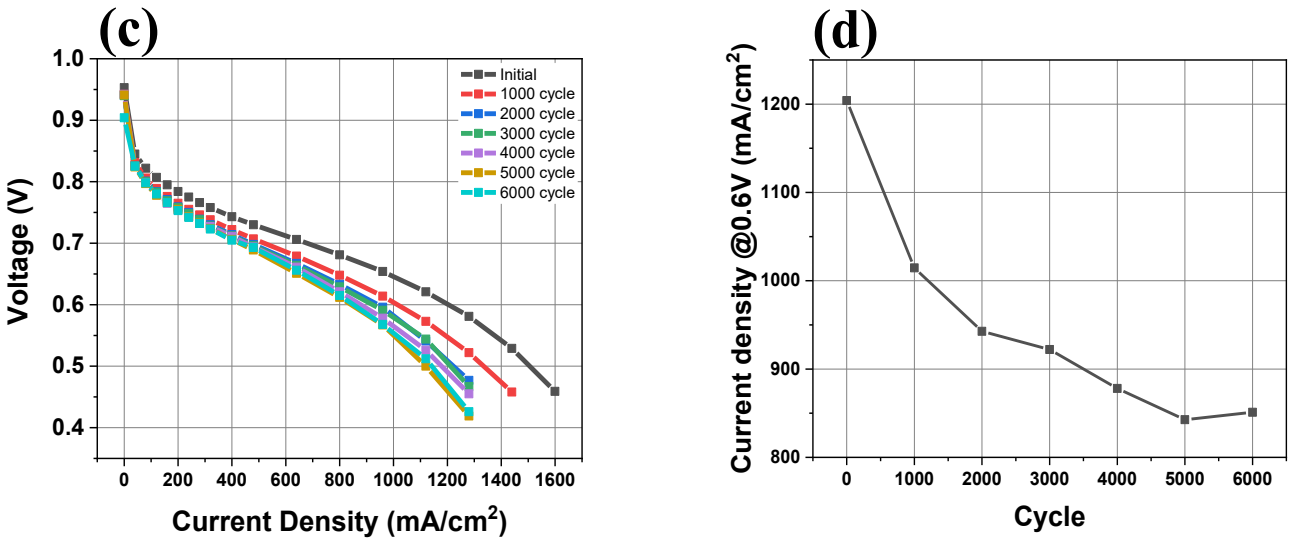


Fig. 3. Variation in (a) CV, (b) ECSA, (c) I-V curve, and (d) current density at 0.6 V with OCV-Wet/Dry Cycle

3.4. Changes in EIS during OCV-Wet/Dry Cycle

Fig. 4 shows the EIS analysis results. Charge transfer resistance (CTR) and high-frequency resistance (HFR) are presented in Fig. 4b and 4c, respectively. The HFR increased up to 5,000 cycles and subsequently decreased after 5,000 cycles. The increase in HFR up to 5,000 cycles is considered to be mainly attributable to an increase in the interfacial contact resistance between the membrane and electrodes caused by repeated swelling and shrinkage under Wet/Dry Cycling conditions.

After the onset of shorting, charge transport through the membrane may occur not only through ionic conduction but also through electron transport, which may lead to a decrease in the overall resistance. HFR observed at 6,000 cycles is considered to be associated with the occurrence of shorting. CTR can be considered to include contributions from the oxygen reduction reaction (ORR) resistance, oxygen transport resistance (OTR), and proton transport resistance (PTR). CTR increased up to 5,000 cycles due to degradation of the cathode catalyst layer. After shorting occurred, electrons passing through the membrane may have affected the cathodic ORR, thereby contributing to the observed decrease in CTR [20, 29].

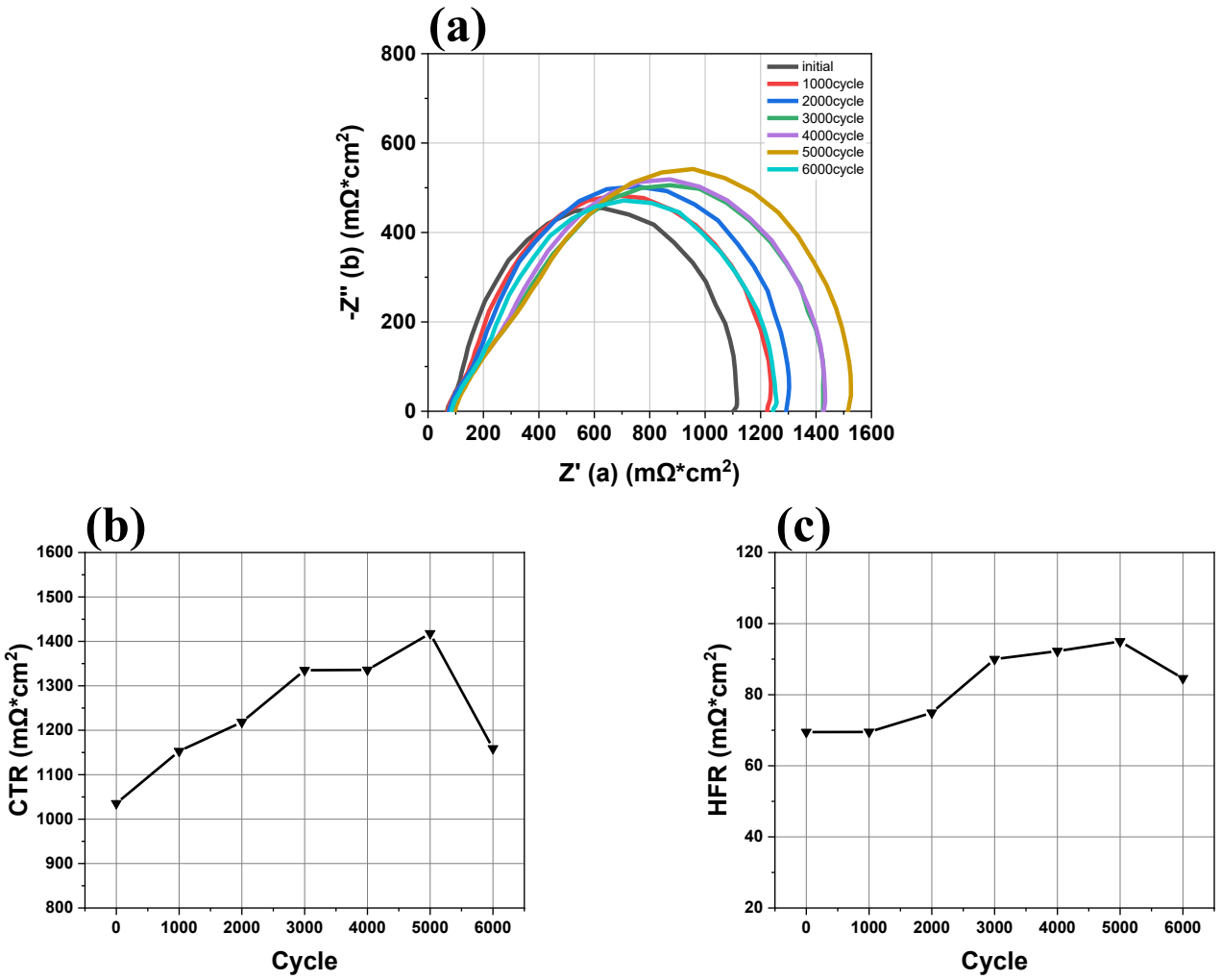


Fig. 4. (a) EIS at 40 mA cm^{-2} and changes in (b) CTR and (c) HFR during OCV-Wet/Dry Cycle

3.4.1 DRT analysis of EIS

Fig. 5 presents the DRT analysis results obtained from the EIS data measured at 40 mA cm^{-2} in Fig. 4. At low current density, the resistance of the catalyst layer is mainly attributed to the oxygen reduction reaction (ORR), which is associated with activation losses arising from the ORR kinetics [26]. In the DRT peak analysis, the oxygen transport resistance was not observed. At low current density, oxygen consumption is relatively small. Therefore, the resistance associated with oxygen diffusion toward the catalyst layer is negligible. and cannot be clearly identified [30]. The ORR resistance (P2) was observed in the frequency range of 5×10^0 to 5×10^1 Hz, whereas the proton transport resistance (P3) appeared in the range of 5×10^1 to 10^3

Hz. In DRT analysis, the behavior of peaks observed at specific frequencies can vary depending on the current density and relative humidity applied during EIS measurements [12, 31].

Fig. 5b shows the evolution of the ORR and proton transport resistance (PTR) during OCV-Wet/Dry Cycle. Both CTR and ORR resistance increased from the initial to 5,000 cycles and then decreased at 6,000 cycles, showing similar trends. The increase in CTR up to 5,000 cycles was mainly attributed to the increase in ORR resistance. This behavior can be explained by irreversible degradation of the Pt catalyst, which reduces ECSA and consequently increases the ORR resistance. The decrease in CTR observed between 5,000 and 6,000 cycles is considered to be associated with the occurrence of shorting. After shorting occurred, electrons passing through the membrane may have affected the cathodic ORR, thereby contributing to the observed decrease in CTR. This interpretation is further supported by the DRT results, which showed that the ORR resistance exhibited the largest decrease between 5,000 and 6,000 cycles.

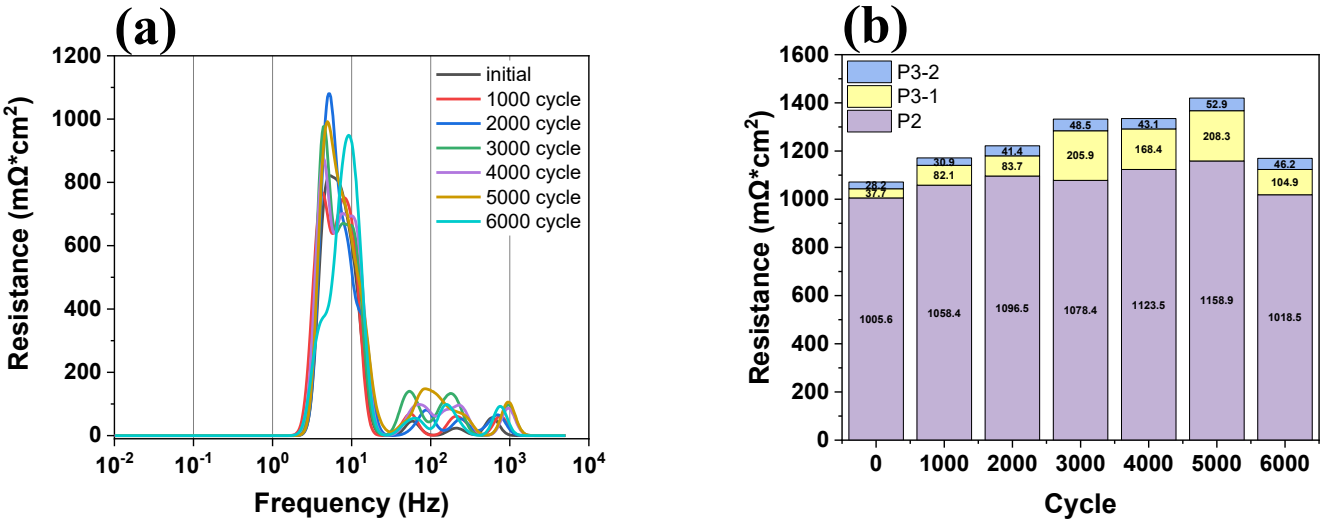


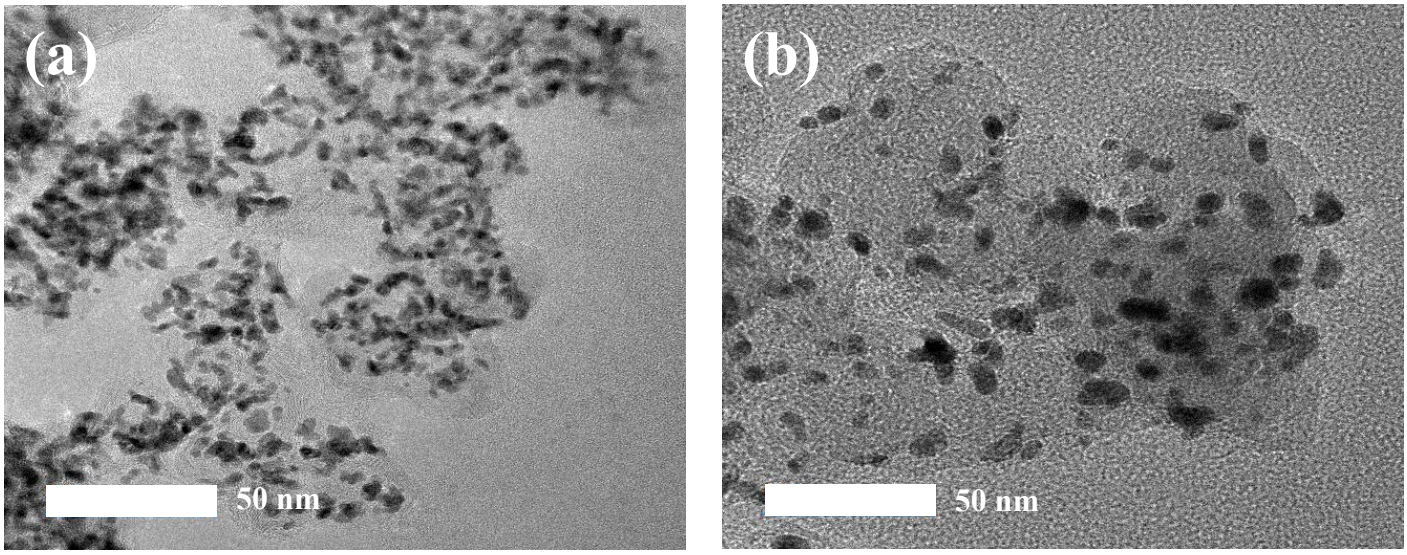
Fig. 5. (a) DRT analysis of EIS at 40 mA cm^{-2}; (b) changes in ORR and PTR peak areas during OCV-Wet/Dry Cycle.

3.5. Pt catalyst particle size analysis using TEM and XRD

Fig. 6 presents TEM images of the pristine and degraded MEAs. The average Pt particle size increased from 3.1 nm in the pristine MEA to 5.5 nm in the degraded MEA, corresponding to an approximately 1.8-fold increase. In the degraded MEA, agglomeration of Pt particles on the

carbon support was clearly observed. Fig. 6c shows the XRD patterns of the pristine and degraded MEAs. The Pt particle size calculated from XRD analysis increased from 2.8 nm before the OCV-Wet/Dry Cycle to 4.8 nm after the cycle, corresponding to an approximately 1.7-fold increase. This result was consistent with the TEM analysis [32].

The observed growth and agglomeration of Pt catalyst particles were attributed to catalyst degradation occurring during OCV-Wet/Dry Cycle. Potential fluctuations during the OCV-Wet/Dry Cycle can induce Pt dissolution. The dissolved Pt species can subsequently redeposit onto existing particles through the Ostwald ripening mechanism. These processes resulted in an increase in Pt particle size and consequently contributed to a decrease in ECSA [16, 33]. Such catalyst agglomeration can also alter the microstructure of the catalyst layer and hinder mass transport within the catalyst layer [31, 34, 35].



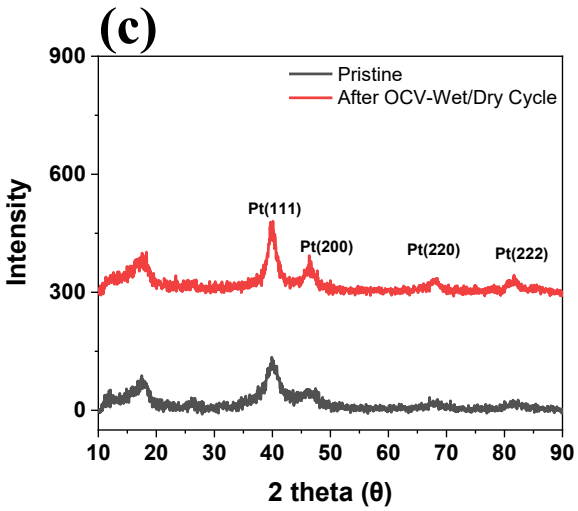


Fig. 6. TEM images and XRD patterns of the MEA before and after OCV-Wet/Dry Cycle: (a) pristine MEA, (b) after degradation, and (c) XRD pattern of the cathode catalyst layer (2θ = 10–90°)

Table 2. Pt Particle Size Before and After OCV-Wet/Dry Cycle

	Pt Particle Size (nm)	
	XRD	**TEM**
Pristine	**2.8**	**3.1**
After degradation	**4.8**	**5.5**

3.6. Cross-Sectional SEM Analysis of the MEA

Fig. 7 presents cross-sectional SEM images of the catalyst layer and membrane of the pristine MEA and the MEA after degradation. Compared with the pristine MEA, a decrease in the thickness of the cathode catalyst layer was observed after degradation. The catalyst layer thickness decreased by approximately 12% relative to that of the pristine MEA. This decrease in thickness was likely associated with the degradation of the catalyst and binder ionomer within the catalyst layer [36]. Dissolved Pt can be lost from the catalyst layer or precipitate within the membrane, while the binder ionomer can be decomposed and removed through

radical-induced degradation. Under these conditions, repeated swelling and shrinkage during Wet/Dry Cycle can impose mechanical stress on the catalyst layer, leading to microstructural changes and a reduction in catalyst layer thickness [23, 36, 37].

The thickness of the electrolyte membrane also decreased by approximately 5% in the degraded MEA compared with the pristine MEA. This membrane thinning is considered to be associated with Pt species generated by catalyst degradation during OCV-Wet/Dry Cycle and subsequently deposited within the membrane. The deposited Pt can promote the formation of radicals within the membrane, which attack the polymer structure of the electrolyte membrane and consequently contribute to membrane thinning [38, 39].

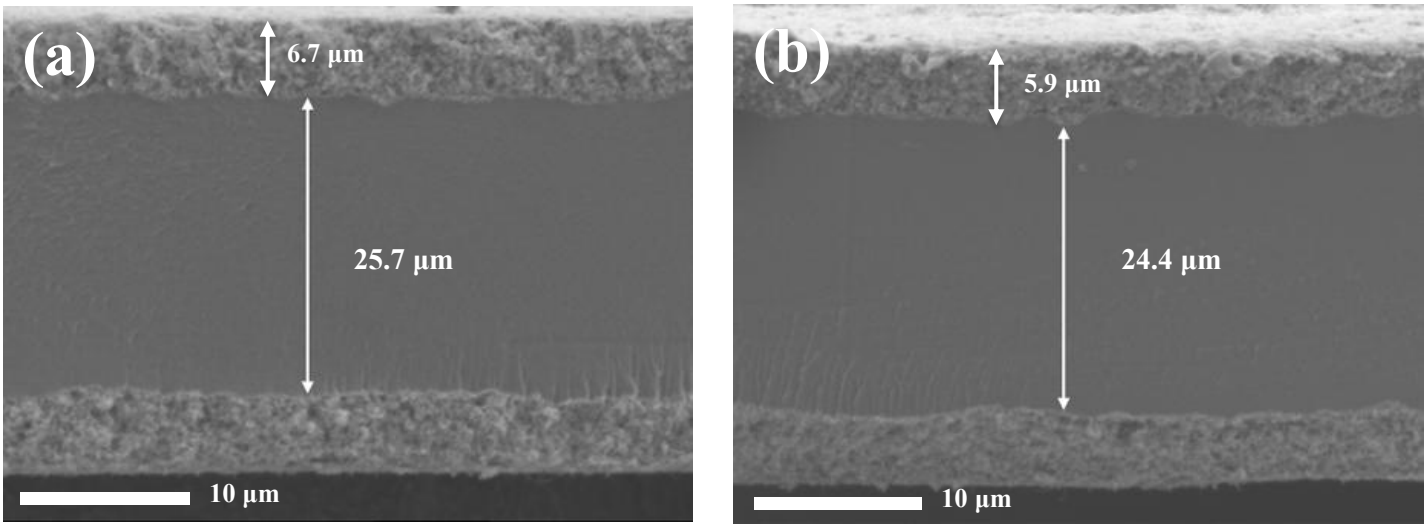


Fig. 7. Cross-sectional SEM images of the MEA before and after OCV-Wet/Dry Cycle: (a) pristine MEA and (b) after degradation

Fig. 8 shows the thermal images of the MEA after degradation. When an internal short circuit forms within the membrane, heat is generated by electron transport through the conductive pathway. Shorting was mainly observed near the cathode inlet and at the edge of the electrode, which is consistent with observations reported in previous studies [20, 40]. The shorting observed at the electrode edge was attributed to an increase in local OCV caused by cathode

overlap, which accelerated the degradation rate of the MEA [41]. The resulting localized thermal damage to the MEA can further increase hydrogen crossover, leading to the expansion of the hot spots. Initially, the high-temperature region was relatively small; however, its temperature increased rapidly, and the region continued to expand even after the hydrogen supply was stopped and replaced with nitrogen. Because the initial shorting area was relatively small, the reduction in I–V performance caused by shorting was also limited.

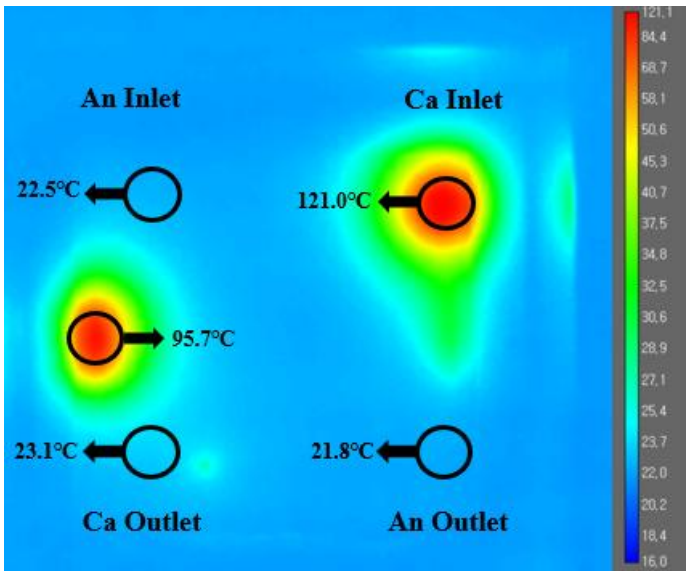


Fig. 8. Thermal imaging analysis of the MEA after OCV-Wet/Dry Cycle

4. Conclusion

In this study, electrode catalyst degradation was investigated during the OCV-Wet/Dry Cycle. The OCV-Wet/Dry Cycle was conducted for 6,000 cycles, and degradation was investigated through electrochemical evaluation and postmortem analysis. During OCV-Wet/Dry cycle, reversible decreases and recoveries in OCV were observed up to 5,000 cycles due to changes in hydrogen crossover and binder-ionomer activity associated with membrane humidification and drying. After 5,000 cycles, however, the OCV behavior became irreversible up to 6,000 cycles, accompanied by a larger voltage fluctuation range. The ECSA gradually decreased up

to 5,000 cycles, whereas the degradation rate increased by approximately fivefold during the irreversible degradation period between 5,000 and 6,000 cycles. The HCCD remained nearly constant up to 5,000 cycles, indicating that significant polymer membrane degradation had not yet occurred. However, HCCD increased sharply during the subsequent irreversible degradation period. This rapid acceleration of membrane degradation can be attributed to radical generation associated with accumulated Pt species within the membrane and to the decrease in SR caused by an increase in short-circuit current. TEM and XRD analyses confirmed that the Pt catalyst particle size increased by approximately 1.7–1.8 times after the AST. In addition, both HFR and CTR decreased after the onset of shorting. DRT analysis further showed that, when shorting occurred, electrons transported through the membrane could reach the Pt catalyst in the cathode catalyst layer and contribute to a reduction in ORR resistance. In addition, shorting was observed through thermal imaging analysis. Consequently, These results indicate that shorting occurred during the OCV-Wet/Dry Cycle as a result of catalyst degradation. These results indicate that catalyst degradation during the OCV-Wet/Dry Cycle led to shorting, resulting in a significant reduction in membrane durability. Therefore, OCV-Wet/Dry cycling should be regarded not only as a membrane degradation test but more appropriately as an MEA chemical/mechanical cycling test in which both the membrane and electrodes undergo degradation.

Acknowledgements This work was supported by the Industrial Technology Innovation Program (00433112, Development of manufacturing technology for high oxygen permeability binder for fuel cell electrodes) funded by the Ministry of Trade, Industry & Energy (MOTIE, Korea).

References

[1] A. Gonzalez-Garay, M. Bui, D. Freire Ordóñez, M. High, A. Oxley, N. Moustafa, P.A. Sáenz Cavazos, P. Patrizio, N. Sunny, N. Mac Dowell, Annu. Rev. Chem. Biomol. Eng., 13 (2022) 501–528.
[2] L. Du, G. Zhang, S. Sun, Automot. Innov., 4 (2021) 131–143.
[3] R. Borup, J. Meyers, B. Pivovar, Y.S. Kim, R. Mukundan, N. Garland, D. Myers, M. Wilson, F. Garzon, D. Wood, P. Zelenay, K. More, K. Stroh, T. Zawodzinski, J. Boncella, J.E. McGrath, M. Inaba, K. Miyatake, M. Hori, K. Ota, Z. Ogumi, S. Miyata, A. Nishikata, Z. Siroma, Y. Uchimoto, K. Yasuda, K.-I. Kimijima, N. Iwashita, Chem. Rev., 107 (2007) 3904–3951.
[4] Y. Xiao, W. Zheng, J. Wang, B. Li, P. Ming, C. Zhang, Applied Energy, 389 (2025) 125759.
[5] L. Birkner, M. Foreta, A. Rinaldi, A. Orekhov, M.-G. Willinger, M. Eichelbaum, Sci. Rep., 14 (2024) 3999.
[6] G. Zhu, Q. Zhang, C. Li, H. Yu, D.A. Cullen, O.C. Marina, Z.-H. Li, D.M. Wayne, J. Xie, Chem Catalysis, 5 (2025) 101303.
[7] P.C. Okonkwo, O.O. Ige, E.M. Barhoumi, P.C. Uzoma, W. Emori, A. Benamor, A.M. Abdullah, Int. J. Hydrogen Energy, 46 (2021) 15850–15865.
[8] V.O. Mittal, H.R. Kunz, J.M. Fenton, Journal of The Electrochemical Society, 154 (2007) B652–B656.
[9] E. Pahon, D. Hissel, N. Yousfi-Steiner, J. Power Sources, 546 (2022) 231895.
[10] S. Oh, D. Lim, Y. Han, S.-T. Lee, D.-G. Yoo, K.-P. Park, Korean J. Chem. Eng., 41 (2024) 545–552.
[11] D.H. Kim, J.G. Kim, H.-S. Jung, C. Pak, Appl. Surf. Sci., 657 (2024) 159797.
[12] M. Heinzmann, A. Weber, E. Ivers-Tiffée, Journal of Power Sources, 402 (2018) 24–33.
[13] S. Lee, S. Oh, D. Yoo, K. Park, Korean Journal of Chemical Engineering, 42 (2025) 157–164.
[14] C. Lim, L. Ghassemzadeh, F. Van Hove, M. Lauritzen, J. Kolodziej, G.G. Wang, S. Holdcroft, E. Kjeang, J. Power Sources, 257 (2014) 102–110.
[15] S.R. Choi, D.Y. Kim, W.Y. An, S. Choi, K. Park, S.-D. Yim, J.-Y. Park, Mater. Sci. Energy Technol., 5 (2022) 66–73.
[16] M. Prokop, M. Drakselova, K. Bouzek, Curr. Opin. Electrochem., 20 (2020) 20–27.
[17] M. Zhao, W. Shi, B. Wu, W. Liu, J. Liu, D. Xing, Y. Yao, Z. Hou, P. Ming, Z. Zou, Electrochimica Acta, 153 (2015) 254–262.
[18] C. Francia, V.S. Ijeri, S. Specchia, P. Spinelli, J. Power Sources, 196 (2011) 1833–1839.
[19] D. Yoo, S. Oh, Y. Han, J. Jeong, S. Jung, K. Park, Korean J. Chem. Eng., 41 (2024) 2433–2440.
[20] F. Ding, X. Zhan, T. Wei, J. Sun, H. Huang, Y. Cui, Z. Shao, Chem. Eng. J., 494 (2024) 153091.
[21] E.F. Johnson, R. Mukundan, A.Z. Weber, Journal of The Electrochemical Society, 173 (2026) 024504.
[22] Q. Wang, H. Xie, B. Dou, W. Zheng, B. Li, J.P. Zheng, X. Li, P. Thondaiman, P. Ming, Appl. Energy, 409 (2026) 127421.
[23] C.G. Chung, L. Kim, Y.W. Sung, J. Lee, J.S. Chung, Int. J. Hydrogen Energy, 34 (2009) 8974–8981.
[24] S. Cherevko, G.P. Keeley, S. Geiger, A.R. Zeradjanin, N. Hodnik, N. Kulyk, K.J. Mayrhofer, ChemElectroChem, 2 (2015) 1471–1478.
[25] G.J.B. Agravante, J.T. Gostick, Journal of The Electrochemical Society, 173 (2026) 074507.
[26] J. Zhang, Y. Tang, C. Song, J. Zhang, H. Wang, J. Power Sources, 163 (2006) 532–537.

[27] S. Zhang, X.-Z. Yuan, J.N.C. Hin, H. Wang, J. Wu, K.A. Friedrich, M. Schulze, J. Power Sources, 195 (2010) 1142–1148.
[28] T. Zheng, J. Xie, R. Zhang, G. Zhao, H. Fan, Y. Feng, S. Wang, J. Wang, W. Ding, J. Power Sources, 647 (2025) 237303.
[29] J. Zhao, H. Liu, X. Li, Electrochem. Energy Rev., 6 (2023) 13.
[30] S. Cruz-Manzo, R. Chen, P. Rama, Int. J. Hydrogen Energy, 38 (2013) 1702–1713.
[31] D. Yoo, S. Park, S. Oh, J.S. Lee, S. Jung, K. Park, J. Power Sources, 663 (2026) 238833.
[32] P.J. Ferreira, G.J. la O', Y. Shao-Horn, D. Morgan, R. Makharia, S. Kocha, H. Gasteiger, Journal of the Electrochemical Society, 152 (2005) A2256–A2271.
[33] Z. Zheng, F. Yang, C. Lin, F. Zhu, S. Shen, G. Wei, J. Zhang, ACS Appl. Mater. Interfaces, 12 (2020) 35088–35097.
[34] D. Yoo, J. Park, S. Oh, S. Park, M.H. Kim, Y. Choi, K. Park, J. Power Sources, 655 (2025) 237902.
[35] P.P. Mukherjee, C.-Y. Wang, Q. Kang, Electrochimica Acta, 54 (2009) 6861–6875.
[36] D. Yoo, S. Park, S. Oh, M.P. Kim, K. Park, Materials, 17 (2024) 4425.
[37] Y. Chang, J. Liu, R. Li, J. Zhao, Y. Qin, J. Zhang, Y. Yin, X. Li, Energy Convers. Manage., 189 (2019) 24–32.
[38] D. Zhao, B. Yi, H. Zhang, M. Liu, J. Power Sources, 195 (2010) 4606–4612.
[39] N. Ohguri, A.Y. Nosaka, Y. Nosaka, J. Power Sources, 195 (2010) 4647–4652.
[40] H. Gunji, M. Eguchi, F. Sekine, Y. Tsutsumi, Int. J. Hydrogen Energy, 42 (2017) 562–574.
[41] B. Sompalli, B.A. Litteer, W. Gu, H.A. Gasteiger, Journal of The Electrochemical Society, 154 (2007) B1349–B1357.